Structure and Resistivity of Bismuth Thin Films Deposited by Pulsed DC Sputtering

S. A. Stanley and M. D. Cropper*

Department of Physics, Loughborough University, Loughborough,
LE11 3TU, United Kingdom.

*Corresponding Author

Bismuth thin films have been deposited using pulsed D.C. magnetron sputter deposition under four deposition conditions; combining powers of 50 W and 100 W and argon gas pressures, 2 mTorr and 10 mTorr. Estimated deposition rates were between 0.08 nm s^{-1} and 3.5 nm s^{-1}. The films were examined using scanning electron microscopy, cross-sectioning using a focussed ion beam (FIB), X-ray diffraction and sheet resistance and Hall Effect measurement. Room temperature deposition gave a predominant orientational texture of (111) rhombohedral. However, higher film thickness, low sputtering power, high sputtering gas pressure and deposition onto a heated substrate above 125°C increases the fraction of (110) orientation. FIB cross-sectioning indicates that films deposited at room temperature have an irregular crystalline structure with voids, but those grown at 160°C are denser with a better polycrystalline structure. Transport measurements indicates a dominance of conduction by electrons, with films deposited at room temperature having high sheet resistance; low sheet resistance being favoured by low sputtering pressure. Deposition at higher temperatures improves the conductivity but increases the Hall coefficient.

Keywords

Magnetron Sputtering; Bismuth; Thin Films; Electrical Measurements; Film Structure.

1. Introduction

Bismuth is an anisotropic semi-metal possessing several unique properties. It has low electron effective mass, large mean free path but low carrier density [1]. Investigations of the element are motivated by fundamental interest, including possible superconductivity, and potential applications such as thermoelectric materials. Bismuth and bismuth containing materials have been made in reduced dimensionality, including nanowires [2] and thin films.

Examples of thin film deposition of bismuth include thermal evaporation [3, 4, 5], molecular beam epitaxy [6], flash evaporation [7], pulsed laser deposition [8, 9] and sputtering by DC [10] and RF [11] potentials. The crystallographic structure and microstructure of these films differs between deposition methods, however most deposition methods do not produce a unique film structure or grain size and the properties of the film can be influenced by deposition parameters. Examples of such parameters include deposition rate, substrate temperature and the process gas pressure in the case of sputter-deposition. The properties of a film may also vary with film thickness.

DC sputtering is a common technique that is used for the deposition of thin films [12]. It offers greater controllability than simple thermal evaporation and has an extra variable in that gas pressure may be controlled separately from deposition rate. Higher pressures tend to thermalise the depositing species, which have a considerably higher energy than evaporated ones, whereas lower gas pressure has less effect; the key parameter being the mean free path. In this paper we report the results of an investigation into the influence of the deposition conditions on the microstructure, texture and electronic properties of bismuth thin films in pulsed D.C. planar magnetron sputtering.

2. Experimental

Bismuth thin films were deposited onto glass substrates using pulsed DC planar magnetron sputtering using a versatile thin films deposition system supplied by PVD Products Inc, Wilmington MA, USA. The system is a stainless steel, clean high vacuum chamber pumped by a two stage system of turbo-molecular pump and rotary pump. The main chamber achieves a base pressure below 2×10^{-8} Torr following a light bake using internal quartz heaters. The base pressure is protected by a load-lock system that enables sample entry without breaking vacuum.

The deposition source was a 3” *PVD Products Titan* planar magnetron in the sputter-up configuration with the axis of the magnetron inclined at an angle of 35° to the vertical and a target-substrate distance of 15 cm. DC power from an *Advanced Energy MDX 1K* supply was used, combined with a *Sparc-LE 20* [13] unit in auto-run mode at 20 kHz to supress arc formation. During deposition, the substrate was rotated at a rate of thirty times per minute to improve film uniformity, the turbo-molecular pump was throttled, and 99.9999% argon was admitted to the chamber under the control of a mass-flow controller.

The films were deposited onto 10 mm × 10 mm glass substrates, which were cleaned both *ex situ* and *in situ*. The external cleaning involved degreasing and drying in acetone, followed by further cleaning in ethanol: each stage accelerated by eight minutes agitation in an ultrasonic bath. Following mounting in the deposition system supported by a recessed Inconel platen, the substrates were subjected to an RF etch in 30 mTorr of argon for thirty seconds at ~0.65 W cm^{-2}.

Before commencing deposition, the vacuum pressure was allowed to fall below 5×10^{-7} mTorr. When deposition was carried out onto heated substrates, the temperature was allowed to equilibrate and the pressure to fall back after the initial out-gassing. The deposition was measured in terms of rates and thickness by an Inficon XTC quartz crystal monitor. The tooling factor for this was determined by producing calibration samples that were evaluated in terms of thickness by both X-ray reflectivity and in a scanning electron microscope edge-on following fracture (in this latter case a silicon substrate was used). Deposition was always carried out in one of four conditions defined by two deposition powers, 50 W and 100 W, and two gas pressures, 2 mTorr and 10 mTorr. The deposition rates given by this were estimated to be: with 50 W, 0.08 nm s^{-1} and 0.10 nm s^{-1} for 2 and 10 mTorr respectively; with 100 W, 2.7 nm s^{-1} and 3.5 nm s^{-1} for 2 and 10 mTorr respectively.

Following deposition, films were examined using scanning electron microscopy (SEM), cross-sectioning using a focussed ion beam (FIB) dual beam system, X-ray diffraction (XRD) and Hall Effect measurement. The SEM images were collected using a Leo 1530FE high resolution field emission gun scanning electron microscope. The FIB system is a Nova 600 Nanolab Dual Beam and comprises a combined high-resolution field emission electron microscope and gallium ion source microscope. XRD analysis of the films utilised an upgraded Philips PW1130 diffractometer in Bragg-Brentano geometry, with a 2θ range of 20-75° and a wavelength of 0.154060 nm from a Cu K_{α} anode.

Electrical measurements of the films were made using an Ecopia HMS-3000/0.55T Hall Effect measurement system, with contacts to the film in *van der Pauwe* geometry. Contacts were made to the corners of the square substrates using silver paste. The system enables straight-forward determination of the sheet resistance and Hall coefficient (with averaging

around the permutations of pairs of connections) by employing a magnetic field of 0.55 T from a permanent magnet.

3. Results and Discussion

3.1 X-ray Diffraction

Four series of films were deposited at room temperature, permuting each of two pressures with two powers. Each series contained films deposited to thicknesses of 20, 50, 100, 200 and 500 nm. XRD scans of these thin films are shown in Figure 1. Bismuth has the rhombohedral structure [14] that is often described as a special case of the hexagonal system. In this report we use the rhomohedral notation. The principal diffraction orders that can be seen in the XRD scans are the (111) at 2θ=22.49°, the (110) at 27.19°, the (211) at 37.9° and the (221) at 44.59°. The relative strengths of these reflections is 3.25, 100, 36.58 and 3.95 respectively for a powder sample [15], though we must bear in mind beam footprint effects when analysing a thin film. The reflection at 45.90° is simply the second order of the (111): the (222). The strength of these diffracted orders indicates that the (111) and (221) orientational textures dominate.

As would be expected, the reflected orders get stronger as the thickness of the film increases, the scans have not been normalised for film thickness. The insets to each of the four panels shows the heights of the four labelled XRD peaks with film thickness denoted by ● for (111), ○ (110), ▼ (211) and ∆ (221). The four exemplar conditions show quite different behaviour. The first thing to notice is that under all deposition conditions the (110) reflection increases proportionately with thickness. The same trend applies to the (211) and (221) reflections. However, in most conditions (except 100 W, 2 mTorr) the strength of the (111) reflection does not increase appreciably after 200 nm.

The influence of deposition conditions on orientation texture is interesting. The conditions have little influence on the (211) and (221) content, but have quite a strong effect on the (110) and (111). It can be seen from Figure 1 (b) and (d) that the higher sputtering pressure favours the (110) orientation, as does lower sputtering power. The (111) orientation, however, is favoured both by the use of high power and low pressure. The prevalence of these two orientations is illustrated more clearly in Figure 2, which shows the ratio of the (110) reflected intensity to that of the (111) in all conditions and for all thicknesses. The behaviour for very thin films is inconclusive, however for films beyond 200 nm the pattern is clear; high gas pressure (open symbols) suppresses the (111) orientation. The orientation textures that we observe in sputtered films are very different from those of thermally evaporated films. In evaporated films deposited at room temperature, the preferred orientation of the crystallites is almost exclusively (111) [3, 5, 6, 16], though elevated substrate temperatures can lead to other orientations [5, 17]. It is perhaps surprising that the higher energy sputtering conditions - low pressure and high power - favour the orientation produced by the low energy technique of evaporation. Figure 2 also confirms that the (110) to (111) ratio is higher for the films deposited at 50 W, but with a lesser effect than the higher gas pressure.

The structure and orientational texture of thin films can be strongly influenced by the temperature of the substrate during deposition. Figure 3(a) shows the evolution of the XRD scans for 500 nm films deposited onto substrates held between 30°C and 175°C. Initial consideration of the figure indicates that there are two different temperature domains here, with the boundary between 110°C and 125°C. Below 110°C the film has a sizeable (111) reflection, but above 125°C the (111) orientation is reduced. Above 125°C, the (110) oriented crystallites are enhanced. Figure 3(b) illustrates this more clearly as it shows the intensity of the four principal reflections with deposition temperature. The enhancement of the (110) reflection at 125°C is quite striking, as a five-fold enhancement in the (110) is accompanied

by a similar reduction in the (111). Above 125°C the strength of the (110) reflection falls away again.

3.2 Electron Microscopy

Direct images of the microstructure of the films have been collected using electron microscopy. The images of the film surfaces deposited at room temperature are quite similar, regardless of deposition conditions. Typical images can be seen in Figure 4. Figure 4(a) shows a magnified image of the 500 nm film deposited at 50 W, 2 mTorr and 0.08 nms^{-1}. The film exhibits a mix of fine grains and hillocks. A poorly developed whisker can be seen to the bottom right, which is a phenomenon that has been reported previously [17, 18, 19, 20] but that grow sparsely at room temperature. From Figure 4(a) it can be seen that the finer grains are typically 100 nm or less whereas the hillocks are around 800 nm across. Figure 4(b) shows an example of a film grown at higher rate, specifically 100 W, 2 mTorr, 0.27 nms^{-1}. The higher rate has made little difference to the gross structure of the film, except that the fine grain size is, perhaps, a little finer. The equivalent films deposited at higher pressure showed little visible difference from those at lower pressure.

These grain sizes observed are consistent with films deposited by other methods. Deposition of films by pulsed laser deposition has been shown to produce micron sized grains [9]. In a study of the temperature dependence of deposition of films at single thickness and single rate by RF sputtering, Kim et al [11] reported 100 nm sized grains but no whiskers. The absence of whiskers there may be due to differences in the deposition apparatus or parameters such as the higher deposition rate, the thinner films produced, or another factor such as plasma impingement on the growing surface.

To investigate the grain structure of the films more carefully, two films were selected for cross-sectioning in the FIB. Figure 5(a-c) shows detail of the film grown at room temperature using 50 W and 10 mTorr to thickness 500 nm and Figure 5(d-f) shows a film grown under the same conditions except a substrate temperature of 160°C. Bismuth melts at 271.3°C which means that the range of temperatures that have been employed here are significant fractions of this. This has implications for the expected film structure, which can be seen from consideration of the zone model proposed by Thornton [21, 22, 23]. Room temperature deposited films are at 0.55 T_m, and those at 160°C are at 0.8 T_m. Thus all our films are deposited in zone 2 or 3 of the zone model, with the room temperature film being nearest to a zone 2 and 160°C being the most clearly zone 3. Films grown in zone 2 are expected to be of dense columnar structure, whereas those in zone 3 will have been modified by bulk diffusion into something resembling polycrystalline films. Thornton's work was for quite thick films, but at 500 nm these films are appreciably thick though the deposition rate used here is much lower.

The FIB cross-sections in Figure 5 require some explanation. In preparation for the cross-section, a thin film of platinum was deposited onto a small area of the film to protect it from sputtering. The area at the edge of the platinum coating was then etched using the gallium ion beam. The effects of this can be seen in the full electron image shown in Figure 5(a), where three distinct layers can be seen toward the bottom of the picture. The dark region at the bottom edge is the cross-section through the glass substrate, the lighter region above is the bismuth thin film and the layer above this is the platinum. Beyond the cross-section of the platinum is the image of the ion-damaged surface.

Looking first at the room temperature deposited film, several features are apparent. In Figure 5(a) the bismuth film can be seen to be polycrystalline with large crystals penetrating

completely through the film, containing some voids. The surface of the film before ion bombardment, shown in Figure 5(b), is the typical mix of smaller and larger grains with some crystals out-growing others. Figure 5(c) shows an enlargement of the film cross-section, with the start of columnar grains typical of zone 2 or the transition zone.

The structure of the film grown at 160°C is quite different. The broad cross-section is shown in Figure 5(d), which reveals a much denser film without voids. The surface of this film is rougher but on a larger length scale than that deposited at room temperature. The surface of this film is shown in Figure 5(e). It is clear that the crystalline structure of the film deposited at 160°C is different from the room-temperature film with more uniformly sized, smoother grains. Features like the one in the centre of the picture, growing out of the film, are quite common. The enlargement of the cross-section, shown in Figure 5(f), reveals the details of the dense grains confirming a zone 3 structure and the beginning of a more three-dimensional polycrystalline structure.

3.3 Transport measurements

Bismuth is a semi-metal with poor conductivity. We have investigated the transport properties of the films using the Hall Effect. The values for the sheet resistance and Hall coefficient, R_H are given in Table 1 for 500 nm films deposited at room temperature under the four conditions employed. The sheet resistance is measured directly and the Hall coefficient is calculated from the usual *van der Pauwe* method [24]. As pure bulk bismuth has equal numbers of holes and electrons, the Hall coefficient is a function of the carrier densities and electron and hole mobilities [25]. Additionally, in thin-film form it is not necessarily the case that the two carriers have equal densities, resulting in the need for fitting magnetoresistance data [4, 16, 26] if charge carrier densities and mobilities are to be determined.

Looking at Table 1, it can be seen that for the sheet resistance the key parameter is the sputtering pressure; the power has little influence. Using a lower argon pressure during sputter deposition produces films with lower sheet resistance. This sheet resistance may be converted into an equivalent bulk resistivity if we make assumptions about uniformity of film thickness and structure. Sheet resistance of 22 $\Omega_{\square}$ yields $\rho=1.1\times10^{-3}$ Ωcm which is much higher than that of bulk bismuth at 1.3×10^{-4} Ωcm [27]. For the films deposited at lower pressure, we get an equivalent resistivity of 8.1×10^{-4} Ωcm, still higher than that of the bulk or of a bismuth whisker [17].

Table 1 also lists the Hall coefficient, and again sputtering pressure is the key parameter; high sputtering pressure gives high Hall coefficient. In every case, the Hall coefficient is negative, suggesting that the density of electrons is higher than the density of holes, but the precise values cannot be determined from this measurement alone. Assuming the Hall coefficient to be largely influenced by the carrier density the data suggests that low sputtering pressure gives higher carrier density, which is consistent with the lowering of sheet resistance. Changes in mobility between low and high sputtering pressure will play a part in these values but this cannot be determined here. Perhaps the mechanism for the increase in carrier density at lower sputtering pressure is increased damage to the film.

The deposition of bismuth at room temperature tends to give films with poor electrical properties [28], so the influence of substrate temperature on the transport properties was investigated. Figure 6 shows the variation of sheet resistance and Hall coefficient with substrate temperature during deposition using a pulsed D.C power of 50 W at 10 mTorr. For temperatures between room temperature and 160°C there is a large fall in sheet resistance. Between room temperature and 90°C the fall is monotonic, but in the region where XRD has revealed that the film texture becomes less predominantly trigonal the resistance increases

slightly. This behaviour is mirrored in the Hall coefficient, which increases with deposition temperature up to 160°C. The increase suggests a fall in carrier concentration as the material quality improves. This indicates that the decrease in sheet resistance is probably driven by an increase in mobility. The final point in the temperature curves, 175°C, indicates degradation in film quality at this temperature. This has been seen previously [11] in post annealed films when at sufficient temperature the film structure changes and disconnects.

4. Summary

Bismuth thin films have been deposited using pulsed D.C. magnetron sputter deposition under different deposition conditions. For deposition at room temperature the predominant orientational textures include (111) and (110). The latter is favoured by higher film thickness, low power and sputtering high gas pressure; deposition onto a heated substrate above 125°C further favours the (110) orientation. The bismuth films deposited at room temperature have fine crystalline grains and hillocks. FIB cross-sectioning indicates that while films deposited at room temperature have an irregular crystalline structure with voids, those grown at 160°C are denser with a better polycrystalline structure. Transport measurements indicates a dominance of conduction by electrons, with films deposited at room temperature having high sheet resistance; low sheet resistance being favoured by low sputtering pressure. Depositing at higher temperatures improves the conductivity but increases the Hall coefficient.

Acknowledgements

John Bates and Geoff West of Loughborough Materials Characterisation Centre are thanked for the SEM and FIB respectively.

References

[1] G. Smith, G. Baraff, and J. Rowell, Phys. Rev. **135**, A1118 (1964).
[2] P. Chiu and I. Shih, Nanotechnology **15**, 1489 (2004).
[3] A. A. Ramadan, A. M. El-Shabiny, and N. Z. El-Sayed, Thin Solid Films **209**, 32 (1992).
[4] M. Inoue, Y. Tamaki, and H. Yagi, J. Appl. Phys. **45**, 1562 (1974).
[5] L. Kumari, S.-J. Lin, J.-H. Lin, Y.-R. Ma, P.-C. Lee, and Y. Liou, Appl. Surf. Sci. **253**, 5931 (2007).
[6] Y. Ahn, Y.-H. Kim, S.-I. Kim, and K.-H. Jeong, Curr. Appl. Phys. **12**, 1518 (2012).
[7] X. Duan, J. Yang, W. Zhu, X. Fan, and C. Xiao, Mater. Lett. **61**, 4341 (2007).
[8] M. Boffoué, B. Lenoir, A. Jacquot, H. Scherrer, A. Dauscher, and M. Stölzer, J. Phys. Chem. Solids **61**, 1979 (2000).
[9] J. C. G. de Sande, T. Missana, and C. N. Afonso, J. Appl. Phys. **80**, 7023 (1996).
[10] J.-H. Hsu, Y.-S. Sun, H.-X. Wang, P. C. Kuo, T.-H. Hsieh, and C.-T. Liang, J. Magn. Magn. Mater. **272-276**, 1769 (2004).
[11] D.-H. Kim, S.-H. Lee, J.-K. Kim, and G.-H. Lee, Appl. Surf. Sci. **252**, 3525 (2006).
[12] D. Depla and S. Mahieu, *Reactive Sputter Deposition* (Springer Science & Business Media, 2008), p. 590.
[13] J. Li, M. K. Narasimhan, V. Pavate, D. Loo, S. Rosenblum, L. Trubell, R. Scholl, S. Seamons, C. Hagerty, and S. Ramaswami, in *Microelectron. Manuf.*, edited by D. N. Patel and M. Graef (International Society for Optics and Photonics, 1997), pp. 33–41.
[14] R. W. G. Wyckoff, *Volume 1*, Second Edition (John Wiley & Sons, New York, 1963), p. 32.
[15] P. Cucka and C. S. Barrett, Acta Crystallogr. **15**, 865 (1962); Powder Diffraction File, Joint Committee on Power Diffraction Standards, ASTM, Philadelphia, PA, 2000, Card 85-1329.
[16] M. Rudolph and J. J. Heremans, Appl. Phys. Lett. **100**, 241601 (2012).
[17] S. A. Stanley, C. Stuttle, A. J. Caruana, M. D. Cropper, and A. S. O. Walton, J. Phys. D. Appl. Phys. **45**, 435304 (2012).
[18] S. Cao, C. Guo, Y. Wang, J. Miao, Z. Zhang, and Q. Liu, Solid State Commun. **149**, 87 (2009).
[19] B.-K. Wu, H.-Y. Lee, and M.-Y. Chern, Appl. Phys. Express **6**, 035504 (2013).
[20] Y. Tian, C. Fei Guo, S. Guo, Y. Wang, J. Miao, Q. Wang, and Q. Liu, AIP Adv. **2**, 012112 (2012).
[21] J. A. Thornton, Annu. Rev. Mater. Sci. **7**, 239 (1977).
[22] J. A. Thornton, J. Vac. Sci. Technol. **11**, 666 (1974).
[23] C. R. M. Grovenor, H. T. G. Hentzell, and D. A. Smith, Acta Metall. **32**, 773 (1984).
[24] L. J. van der Pauw, Philips Res. Repts. **13**, 1 (1958).
[25] Y. Hasegawa, Y. Ishikawa, T. Saso, H. Shirai, H. Morita, T. Komine, and H. Nakamura, Phys. B Condens. Matter **382**, 140 (2006).
[26] A. H. de Kuijper and J. Bisschop, Thin Solid Films **110**, 99 (1983).
[27] C. F. Gallo, B. S. Chandrasekhar, and P. H. Sutter, J. Appl. Phys. **34**, 144 (1963).
[28] B. Y. Jin, H. K. Wong, G. K. Wong, J. B. Ketterson, and Y. Eckstein, Thin Solid Films **110**, 29 (1983).

Figure Captions

Figure 1: X-ray diffraction with thickness from the bismuth thin films deposited by pulsed D.C. magnetron sputtering in four series: (a) 50 W 2 mTorr; (b) 50 W 10 mTorr; (c) 100 W 2 mTorr; (d) 100 W 10 mTorr. The intensity of the four principal reflections is shown in the insets.

Figure 2: Plot of the ratio of the intensities of the (110) and (111) reflections with film thickness for bismuth thin films deposited by pulsed D.C magnetron sputtering under the four different conditions.

Figure 3: X-ray diffraction with deposition temperature for pulsed D.C. deposited bismuth thin films. Panel (a) shows the scan in Bragg-Brentano geometry, (b) shows the intensities of the four principal reflections, (c) shows the ratio of the intensities of the (110) and (111) reflections.

Figure 4: Scanning electron microscope images of bismuth thin films deposited using pulsed D.C. at 2 mTorr argon pressure: (a) at 50 W to give a rate of 0.08 nms^{-1} and (b) at 100 W to give 0.27 nms^{-1}.

Figure 5: Focussed ion beam cross-sections through films deposited using pulsed D.C deposition at 10 mTorr argon pressure and 50 W to give a rate of 0.1 nms^{-1} at two different substrate temperatures: room temperature (a-c) and 160°C (d-f).

Figure 6: Transport properties with deposition temperature for pulsed D.C. deposited bismuth thin films using 50 W at 10 mTorr. Panel (a) shows the sheet resistance and (b) shows the Hall coefficient, R_H.

Figure 1

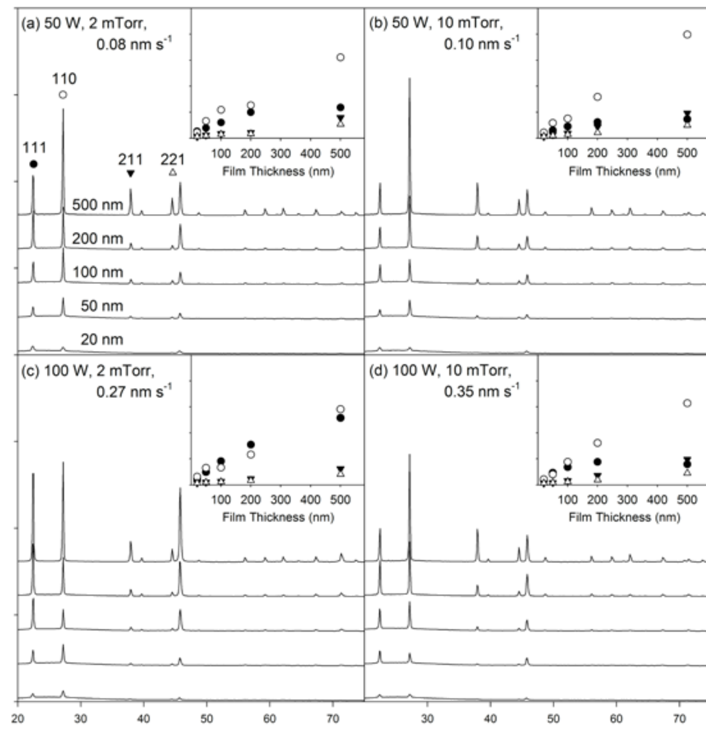

Figure 2

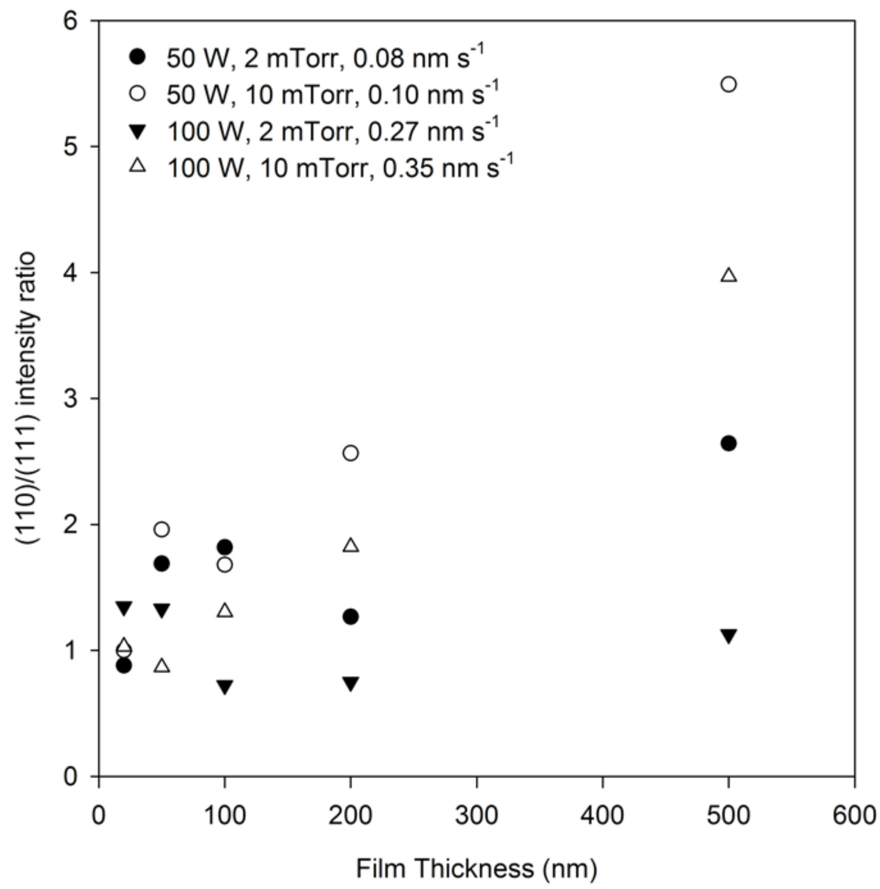

Figure 3

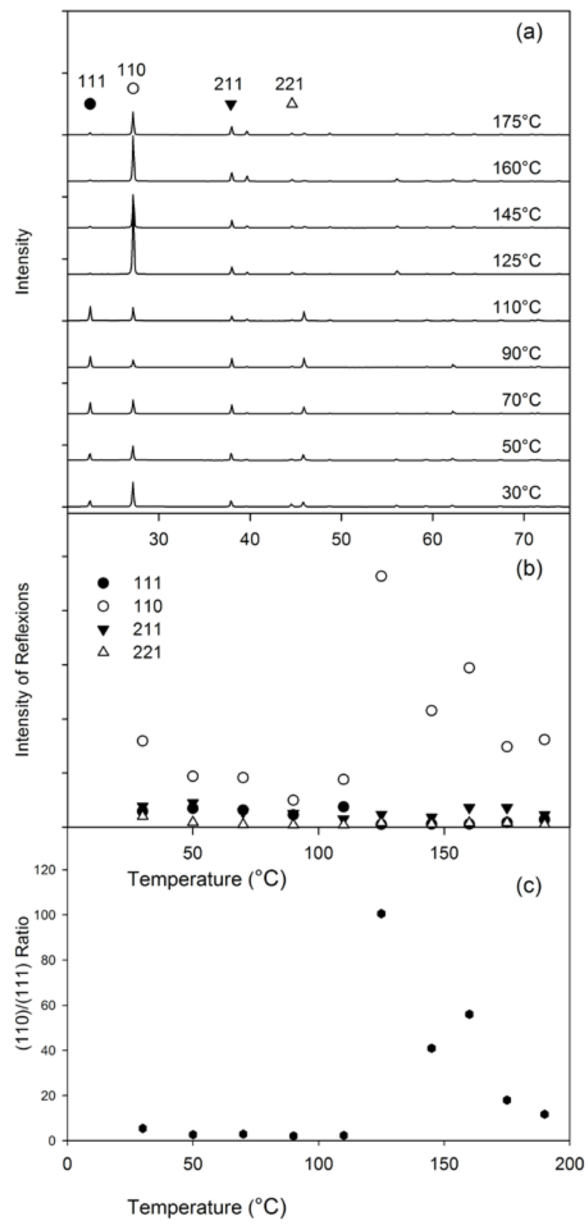

Figure 4

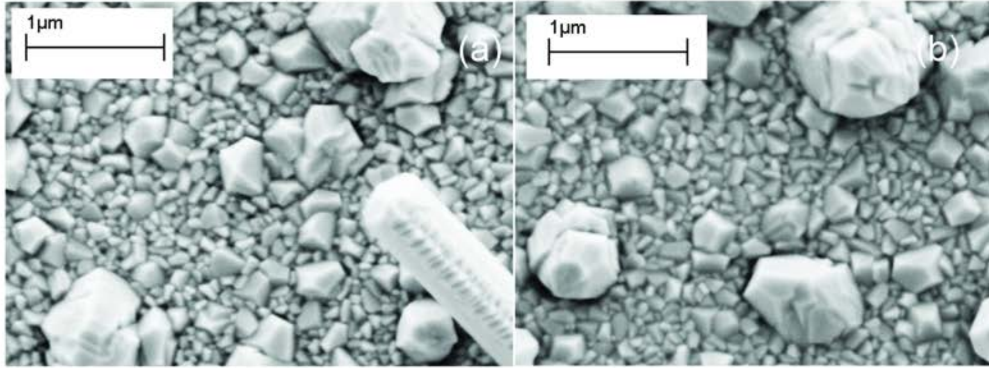

Figure 5

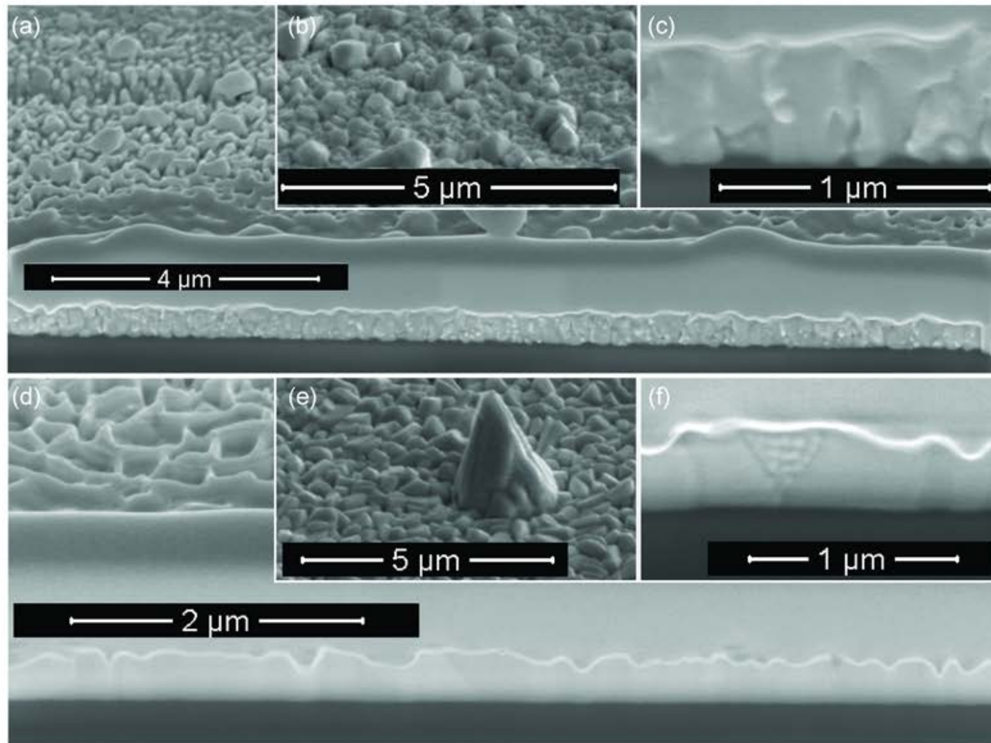

Figure 6